Atmos. Chem. Phys., 20, 475–485, 2020
https://doi.org/10.5194/acp-20-475-2020

Atmospheric Chemistry and Physics
Open Access
EGU

Simulation of mixed-phase clouds with the ICON large-eddy model in the complex Arctic environment around Ny-Ålesund

Vera Schemann and Kerstin Ebell

Institute of Geophysics and Meteorology, University of Cologne, Cologne, Germany

Correspondence: Vera Schemann (vera.schemann@uni-koeln.de)

Received: 24 June 2019 – Discussion started: 27 June 2019
Revised: 5 November 2019 – Accepted: 8 November 2019 – Published: 14 January 2020

Abstract. Low-level mixed-phase clouds have a substantial impact on the redistribution of radiative energy in the Arctic and are a potential driving factor in Arctic amplification. To better understand the complex processes around mixed-phase clouds, a combination of long-term measurements and high-resolution modeling able to resolve the relevant processes is essential. In this study, we show the general feasibility of the new high-resolution icosahedral nonhydrostatic large-eddy model (ICON-LEM) to capture the general structure, type and timing of mixed-phase clouds at the Arctic site Ny-Ålesund and its potential and limitations for further detailed research. To serve as a basic evaluation, the model is confronted with data streams of single instruments including a microwave radiometer and cloud radar and also with value-added products like the CloudNet classification. The analysis is based on a 11 d long time period with selected periods studied in more detail focusing on the representation of particular cloud processes, such as mixed-phase microphysics. In addition, targeted statistical evaluations against observational data sets are performed to assess (i) how well the vertical structure of the clouds is represented and (ii) how much information is added by higher horizontal resolutions. The results clearly demonstrate the advantage of high resolutions. In particular, with the highest horizontal model resolution of 75 m, the variability of the liquid water path can be well captured. By comparing neighboring grid cells for different subdomains, we also show the potential of the model to provide information on the representativity of single sites (such as Ny-Ålesund) for a larger domain.

1 Introduction

The Arctic is warming at a higher rate than the global mean: the increase in the near-surface air temperature in the Arctic is more than twice as large as the observed increase in global mean temperature (Serreze and Barry, 2011; Wendisch et al., 2017). In order to better understand this phenomenon called Arctic amplification, many efforts are currently being undertaken to pinpoint and quantify the related feedback mechanisms causing the enhanced climate change signal (e.g., Wendisch et al., 2017; Screen et al., 2018; Goosse et al., 2018). Low-level mixed-phase clouds are known to be one potential driver of Arctic amplification and are very common in the Arctic (Shupe et al., 2008), but, especially under Arctic conditions, many climate models struggle to capture these clouds depending on their microphysics parameterization (Pithan et al., 2014) and to represent the boundary layer structure due to low and strong inversions. To improve the relevant parameterizations in climate models, a better process understanding and formulation is necessary and can be obtained by creating a synthesis of state-of-the-art observations and high-resolution process modeling.

Concerning observations, enhanced measurement capabilities during specific campaigns can be of great value (e.g., Wendisch et al., 2019; Tjernström et al., 2019; Shupe et al., 2006). In particular, the upcoming Multidisciplinary drifting Observatory for the Study of Arctic Climate (MOSAiC) campaign (https://www.mosaic-expedition.org/, last access: 11 December 2019) will provide, for the first time, continuous observations of the atmosphere, ice and ocean in the central Arctic over a full year. While they provide a wealth of information about the central Arctic from various instrumentation, such campaigns are always limited to a certain time period. However, in order to understand a changing climate,

long-term measurements are crucial. Such observations are made at the French–German Arctic research station AWIPEV in Ny-Ålesund, Svalbard (78.925° N, 11.930° E). Ny-Ålesund is located on the southern coast of the Kongsfjorden and is surrounded by glaciers and mountains which affect the local climate (Maturilli et al., 2013; Maturilli and Kayser, 2017). AWIPEV operates comprehensive and state-of-the-art instruments for thermodynamic, aerosol, trace gas and surface radiation observations in particular. Some of the observations were started more than 30 years ago, thus enabling trend analyses (Maturilli et al., 2015; Maturilli and Kayser, 2017). In 2016, a frequency-modulated continuous wave 94 GHz Doppler cloud radar of the University of Cologne (Küchler et al., 2017) was installed at AWIPEV, providing highly temporally and vertically resolved cloud observations and enabling the analysis of microphysical processes of Arctic clouds in more detail at this site (Nomokonova et al., 2019; Gierens et al., 2019).

The complex surroundings of Ny-Ålesund create their own need for high-resolution simulations that can capture the surface heterogeneities caused by the mixed surroundings of mountains, flat land, glaciers and the fjord. These conditions mean that the conventional idealized way to run large-eddy simulations with periodic boundary conditions and homogeneous surfaces is not feasible (e.g., Klein et al., 2009; Ovchinnikov et al., 2014; Loewe et al., 2017). For this reason, we have applied the new icosahedral nonhydrostatic large-eddy model (ICON-LEM) for the first time in the Arctic. So far the model has been mainly applied over Germany (Heinze et al., 2017; Marke et al., 2018), showing a reasonable representation of clouds and turbulence. Thus, our main research question is if the ICON-LEM can reproduce the general structure of the observed mixed-phase clouds at Ny-Ålesund by taking into account the complex topography. Beyond the general classification, we also investigate how suitable the default microphysics and especially the parameterizations of cloud condensation nuclei (CCN) and ice nuclei (IN) (Hande et al., 2016) are for the Arctic regime. To investigate these questions, we picked an 11 d long time period (14 to 24 June 2017) during the ACLOUD and PASCAL campaigns (Wendisch et al., 2019), when, in addition to the ground-based observations, aircraft-based remote sensing and in situ observations were also performed in the surroundings of Ny-Ålesund. These observations will be used in further analysis in the future.

The advantage of a large-eddy simulation is that we can simulate at temporal and spatial scales that are comparable to the observations. However, due to computational costs, we always have to find a balance between resolution and domain size. A rather small and limited domain comes with the need for large-scale forcing to capture the general synoptic situation. For this reason, forcing from numerical weather prediction models has to be applied to obtain information about the synoptic situation and the large scales. As the large-scale models struggle with the Arctic conditions and especially the inversion strength (e.g., Pithan et al., 2014; Neggers et al., 2019), forcing from two different weather prediction models (Integrated Forecasting System (IFS) of the European Centre for Medium-Range Weather Forecasts (ECMWF) and the ICON global model of the German Meteorological Service (DWD); Zängl et al., 2015) has been used. The transition from large-scale forcing to high-resolution simulations is a well-known difficulty: inconsistent forcing might introduce artifacts in the high-resolution simulations or need very long spin-up times. This problem is mitigated by the new ICON model suite, which enables consistent forcing throughout the whole model hierarchy. We can use the operational weather forecast simulations and force our large-eddy model to maintain a consistent atmospheric state and a model setup where only the respective parameterizations are switched off or are replaced by a more suitable version (e.g., for turbulence). We will show how beneficial this feature of the ICON family is and also look into the effect of increasing the horizontal resolution.

In this study, we demonstrate the general applicability of ICON-LEM in the Arctic, in particular in a place with a complex topography, to evaluate and study clouds. After a description of the general model setup (Sect. 2.1) and the observations used (Sect. 2.2), we will tackle our main research questions, which are as follows:

- Can the ICON-LEM capture the general structure of mixed-phase clouds at Ny-Ålesund, as characterized by the CloudNet classification (Sect. 3)?
- Is the consistent forcing within one model family beneficial (Sect. 4.1)?
- Are the default microphysical parameterizations and a horizontal resolution of 75 m suitable for Arctic conditions (Sects. 5 and 5.2)?
- Can we use high-resolution simulations to evaluate the representativity of point measurements at complex locations (Sect. 5.3)?

2 Setup

2.1 Model simulations

The large-eddy model of the ICON modeling system was developed during the High-Definition Clouds and Precipitation for Advancing Climate Predictions ($HD(CP)^2$) project and was successfully tested and evaluated over Germany (Dipankar et al., 2015; Heinze et al., 2017). In this study, we show the first application of this model in the Arctic, facing the difficult terrain and surface conditions around Ny-Ålesund. The setup consists of four different domains with one-way nesting. The largest domain has a horizontal resolution of 600 m, a 3 s time step and a domain size of 110 km. The smallest domain has a 75 m resolution, a 3/8 s time

step and a domain size of 25 km (Fig. 1). Due to the triangular grid, resolution in this context means edge length, which actually gives a 2/3 higher resolution when using the traditional definition in which resolution is the root of the cell area. The vertical resolution is the same for all horizontal resolutions and is highest close to the surface. The average vertical resolution between 500 m and 1.5 km is approximately 68 m. For the 11 d period between 14 and 24 June 2017, every day is simulated separately with a new initialization at 00:00 UTC. The simulations are performed with the two-moment microphysics scheme from Seifert and Beheng (2006) including six prognostic hydrometeors (water vapor, cloud water, cloud ice, rain, snow, hail and graupel) and a Smagorinsky turbulence scheme (Dipankar et al., 2015). The CCN and IN are described following a parameterization based on Hande et al. (2016). Due to the relatively small domain, the large-scale forcing is very important for capturing the general synoptic situation. The forcing is applied only at the boundaries so that the flow can evolve and develop freely in the inner part of the domains. Nevertheless, the simulations depend on the large-scale forcing and different forcing models can lead to different results. For this reason, we use two different models, the IFS model with a horizontal resolution of $0.1^\circ \times 0.1^\circ$ and the ICON global model with the R3B7 (approximately 13 km) resolution, and investigate the differences. A new forcing file is imported every 1 h for the IFS model and every 3 h for the ICON global model. While the IFS data profit from a rather high resolution due to the fact that our study region is close to the pole, the ICON resolution stays constant due to the triangular grid structure at approximately 13 km, which is too coarse to force the ICON-LEM directly. For this reason, we introduced an intermediate step with approximately 2 km horizontal resolution and adjusted parameterizations (ICON-NWP) to be similar to the global simulations (see Fig. 1a).

For the main part of the analysis, we use the so-called meteogram output, which is the column output at the grid cell closest to the coordinates of the Ny-Ålesund measurements. The output is written every 9 s, which brings it close to the temporal resolution of the observational data sets. Due to the included topography and open boundaries, we expect the column to be representative of the conditions in Ny-Ålesund and thus to provide a better estimate than traditional quantities like the domain mean or variance. Additionally, the weather is often driven by large-scale conditions and further affected by local topography and surface conditions which are accounted for in the ICON-LEM. Nevertheless, these point-to-point comparisons can cause further uncertainties for observation model comparisons, e.g., by missing clouds or certain structures which might be represented in neighboring cells. For this reason, we also included the two-dimensional output of the liquid water path (LWP) in our analysis, which has been recorded at 10 min intervals.

2.2 Observational data set

The model simulations are compared to observations performed at the atmospheric observatory of the French–German Arctic research station AWIPEV in Ny-Ålesund. In this study, we use information from microwave radiometer and cloud radar observations and from a synergistic classification product.

The 94 GHz Doppler cloud radar of the University of Cologne (Küchler et al., 2017; Nomokonova et al., 2019) provides vertical profiles of cloud radar reflectivity factor Z, Doppler velocity and spectral width up to a height of about 12 km. In this study, we make use of the cloud radar reflectivity profiles which have been brought to a common 30 s and 20 m temporal and height grid, respectively. In addition to the active component, the cloud radar also has a passive channel at 89 GHz. The brightness temperatures measured at 89 GHz were used to retrieve the LWP, as described in the next paragraph.

Information on integrated water vapor (IWV) and the LWP was taken from the Humidity And Temperature PROfiler (HATPRO) at AWIPEV, which is a 14-channel microwave radiometer (MWR). Details on the HATPRO retrievals can be found in Nomokonova et al. (2019). The 1 s MWR measurements were averaged onto a common 9 s temporal grid similarly to the ICON-LEM output. Since the HATPRO was not measuring between 21 and 24 June and had also a few data gaps on other days, we took additional LWP information from a statistical retrieval based on the additional passive 89 GHz channel of the cloud radar. For this LWP retrieval, we combined 89 GHz brightness temperature measurements with IWV information from GPS. In cases where the HATPRO LWP is not available but the LWP from the 89 GHz retrieval is available, the latter is used, resulting in a combined, best-estimate data set for the LWP. For the analysis of the power spectrum, continuous data are crucial. We thus divided the time series into 6 h intervals and excluded from the analysis those intervals which still suffered from data gaps.

While the cloud radar reflectivity profiles provide information on the vertical occurrence of hydrometeors, more detailed information on hydrometeor type is provided by the CloudNet target classification product (Illingworth et al., 2007; Nomokonova et al., 2019). For this classification, each radar height bin is classified with respect to the occurrence of cloud liquid droplets, ice, melting ice and drizzle/rain, and finally the profiles of cloud radar reflectivity, Doppler velocity and ceilometer attenuated backscatter are combined with numerical weather prediction data. The resulting classification profiles have the same temporal (30 s) and vertical (20 m) resolution as the cloud radar measurements.

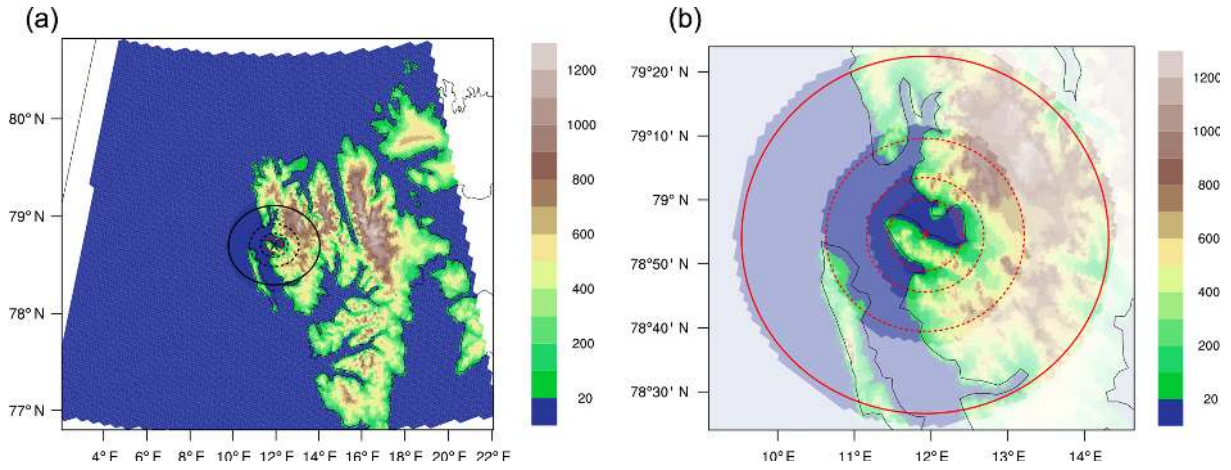

Figure 1. The topography (m), domain size and resolution around Ny-Ålesund for the 2 km ICON-NWP simulation **(a)** and the nested ICON-LEM simulations **(b)**. The circles indicate the model domains for the 600, 300, 150 and 75 m horizontal resolution model runs, respectively (from outer to inner circle) with corresponding domain sizes of approximately 110, 60, 35 and 25 km.

3 Basic evaluation of clouds

We use the CloudNet target classification for an initial assessment of the general representation of structure, type and timing of the modeled versus the observed clouds. The CloudNet classification also provides an impression of the changing meteorological conditions, e.g., the occurrence of frontal passages or low-level mixed-phase clouds. The classification of the model output is based on a threshold of $10^{-8}\,\mathrm{kg\,kg^{-1}}$ for the hydrometeors and shows reasonable agreement (Fig. 2) with the CloudNet classification described in the previous section. The general situation is mostly captured by the models, and also type, structure and timing are represented well. Nevertheless, some differences, especially in the duration of mixed-phase clouds, can be spotted immediately. With regards to resolution, the 2 km resolution shows reasonable agreement even though it has a tendency to generate more precipitation; however, it also shows that the large-eddy simulation benefits from a good representation of large-scale atmospheric forcing in the numerical weather prediction data.

The variability of the atmospheric conditions during the 11 d has already been indicated by the CloudNet classification but can also be seen in the time series of the IWV and the LWP (Fig. 3). For the IWV (Fig. 3a), both resolutions nicely follow the observed general trend. As the IWV is mainly dominated by larger scales, hardly any difference can be seen between the lowest (600 m) and highest (75 m) horizontal resolution. Strong gradients often occur at 00:00 UTC, which are due to the new model initialization at this time. The model output between 00:00 and 06:00 UTC should be treated with caution as it includes the model spin-up but is shown here for completeness. For the LWP (Fig. 3b), the models also capture most of the clouds and variability even though some clouds are missing, which could already be seen in the classification (Fig. 2). For the LWP, the two different ICON-LEM resolutions deviate from each other. These differences are analyzed and shown in more detail in Sect. 5.2.

4 The 23 June 2017 case study

The previous section showed that the 2 km forcing data already capture the general structure, type and timing of the clouds during the analyzed time period. The very similar classification time series of the ICON-LEM and ICON-NWP simulations indicate that the representation in the ICON-LEM is strongly influenced by the forcing data. We will thus investigate the forcing dependency in more detail by focusing on 23 June 2017, which reveals a complicated cloud structure with a very thin mixed-phase cloud and several liquid layers.

4.1 Forcing dependency

The 23 June 2017 case is a very strong example of the impact of different forcing models on the representation of mixed-phase clouds in the ICON-LEM. Figure 4a–c show the hydrometeor classification on this day for the observations and the ICON-LEM and also for the 75 m output of the ICON-LEM forced by IFS data. Figure 4d–f show the forcing data itself. While the ice cloud is represented in all forcing data, it is evaporated immediately and not fully recovered in the ICON-LEM simulation forced with the IFS data. The reason for the sudden evaporation is probably a different set of parameterizations and the relation between subgrid-scale (ice) clouds and the mean state in the models. The transition to a different state representation in the ICON model leads to a mismatch. The ICON-LEM with a 75 m resolution and forced by the ICON model chain captures the cloud situation with low- and midlevel mixed-phase clouds and higher ice cloud in the afternoon much better than the one forced with

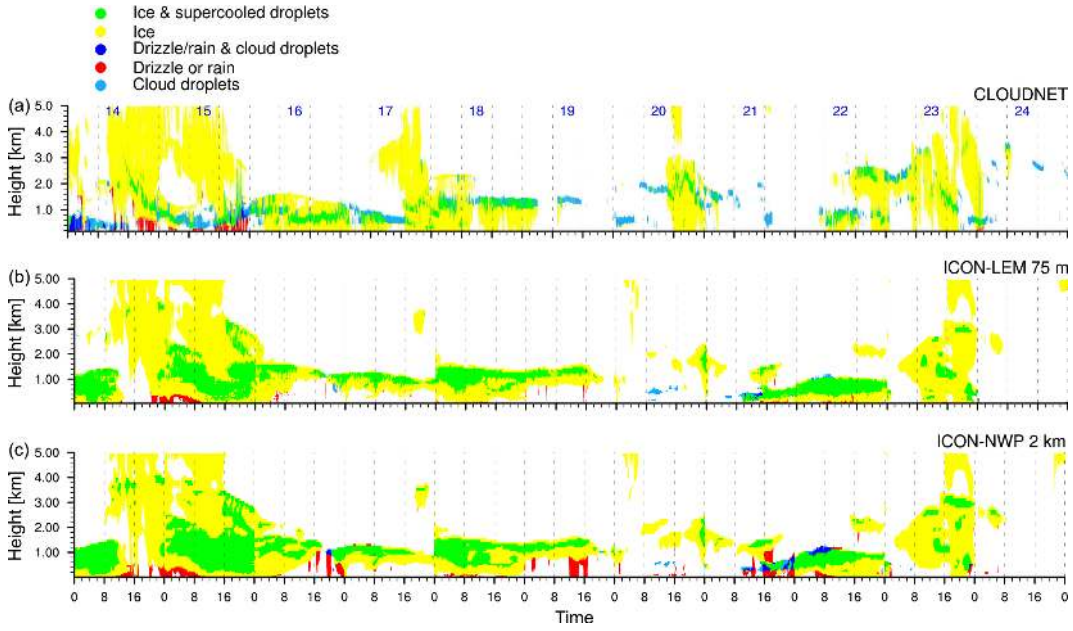

Figure 2. Hydrometeor classification for the whole time series for the observations **(a)**, the ICON-LEM 75 m simulation **(b)** and the ICON-NWP 2 km forcing data **(c)**.

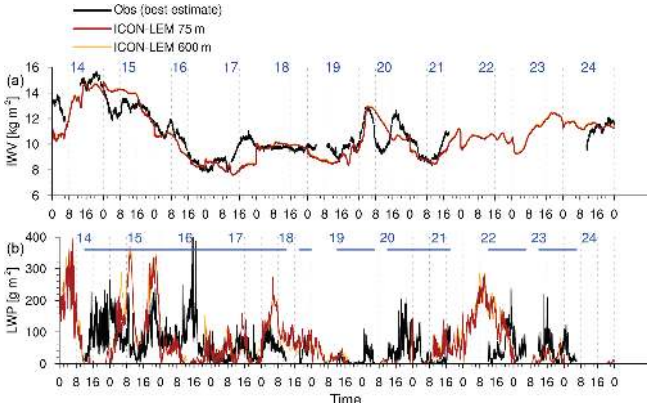

Figure 3. Time series of observed (black) and of ICON-LEM simulated (600 m, yellow; 75 m, red) IWV **(a)** and LWP **(b)**. Blue lines show data availability of the observations.

the IFS data. The mixed-phase clouds at around 2 km height at the beginning of the day are not captured by the ICON-LEM possibly because of the spin-up time of the model. This example shows the importance of applying consistent forcing data, which is possible with the new ICON suite that can simulate at scales ranging from climate scales to large-eddy-resolving scales.

4.2 Vertical structure of the clouds

While the general structure is captured in the ICON-LEM simulation with the ICON forcing, we are also interested in the composition of the clouds and the dominating microphysical properties and processes. On the one hand, cloud properties which have been retrieved from observations could be directly compared to the model results. However, retrieval algorithms applied to measurements may induce large uncertainties in this comparison. On the other hand, the modeled mixed-phase cloud properties can be evaluated by comparing observed cloud radar reflectivities with forward-simulated reflectivities based on the ICON-LEM output. Figure 5 shows the observed reflectivities as well as those from the ICON-LEM which were forward simulated with the Passive and Active Microwave TRAnsfer (PAMTRA) model (Maahn et al., 2015). Radar reflectivity depends on both hydrometeor concentration and size. We consistently find that the simulated reflectivities are lower than the observed ones. This underestimation might indicate that the ICON-LEM clouds consist of particles that are too small. One possible explanation could be the limitation of the CCN and IN parameterizations applied. Another issue could be in the description of growing processes for the ice clouds.

5 Statistical evaluation

While case studies allow us to investigate certain situations in detail, they might not be representative of the general model behavior. In this section, we use all 11 d to tackle the questions of how well the microphysical composition of the clouds is represented in the simulations and how much information can be added by using higher horizontal resolutions.

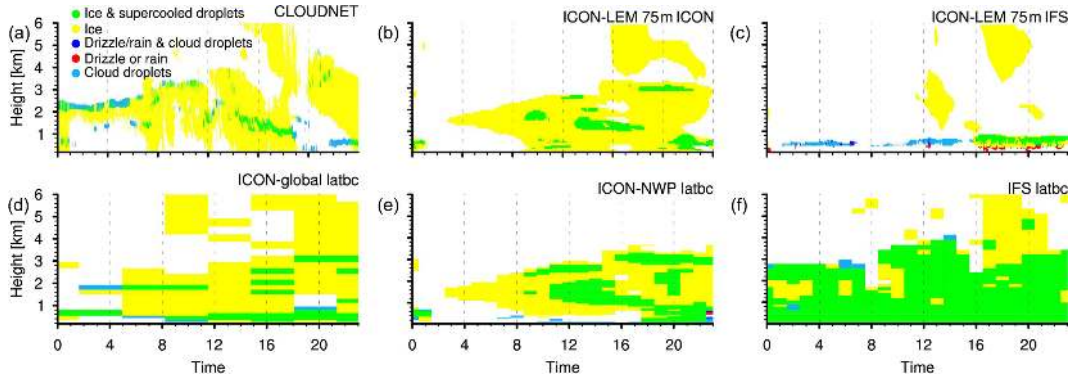

Figure 4. Classification for the case study of 23 June 2017 showing the observations **(a)** the ICON-LEM results at 75 m resolution with forcing from the ICON family **(b)** and the ICON-LEM results at 75 m resolution with forcing from the IFS **(c)**. The respective forcing data for the lateral boundary conditions (latbc) from the ICON global model (ICON-global; **d**), the ICON at 2 km resolution (ICON-NWP; **e**) and the IFS **(f)** are also shown.

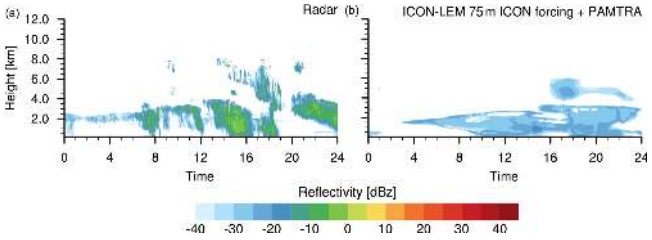

Figure 5. Time series of observed **(a)** and simulated cloud radar reflectivity based on the ICON-LEM with 75 m resolution **(b)** for the case study of 23 June 2017.

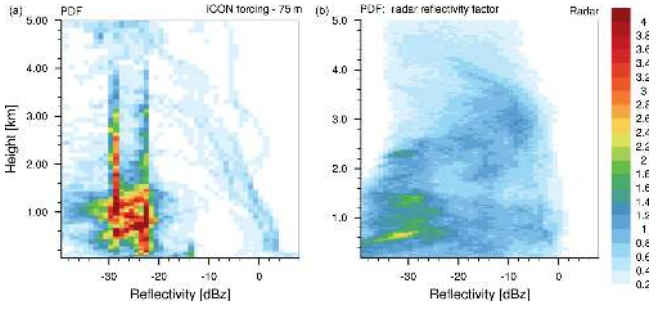

Figure 6. 2-D histogram for simulated **(a)** and observed **(b)** radar reflectivities for all 11 d (14–24 June 2017). The PDF (%) of each height is based on the maximal possible number of data points (normalized).

5.1 Reflectivity distribution

As the ice cloud on 23 June 2017 is very thin and challenging for the model (as seen in the previous section), the underestimation of the radar reflectivity might not be representative of the general model behavior. We thus compare the observed and simulated reflectivities for all 11 d in a 2-D histogram (Fig. 6). The frequencies are based on the total number of possible data points (e.g., 9600 for the model output). With this approach, the distributions provide information about the total frequency at all heights simultaneously. Interestingly, in the model radar reflectivities are basically confined to values between −32 and −20 dBZ with two distinct peaks around −29 and −23 dBz. Up to 1.5 km in height, observed radar reflectivities range between −36 and −24 dBZ. Such a higher occurrence of radar reflectivities can also be seen in the model. The histogram confirms the results of the case study that the simulated reflectivities tend to be too low compared to the observed ones. This becomes even more clear for the clouds at around a 3 km height, where the observed frequencies shift toward higher values, while the simulated ones stay close to −30 dBz. However, the observed and the simulated reflectivities cover in principal the same range, indicating the potential to reach a better representation by refined microphysical parameterizations. The occurrence of simulated low radar reflectivities that is too high and the two distinct peaks coincide with very small and persistent ice water content (not shown) and might be due to overestimated ice nuclei (IN) and cloud condensation nuclei (CCN) number concentrations. In order to better explain the differences between simulated and observed radar reflectivities, more detailed sensitivity studies are needed that disentangle the effects of CCN, IN and microphysical processes. This will be part of future research with upcoming long-term measurements of IN and CCN.

5.2 Resolution dependency

When looking at the general representation of the cloud structure as given by the hydrometeor classification (Fig. 2), the difference between different resolutions of the ICON model was rather small. In this section, a more detailed analysis of the impact of the different resolutions will be presented. The analysis is performed on the meteogram output, which has an output frequency of 9 s and approaches the temporal scale of the observations. Being able to compare obser-

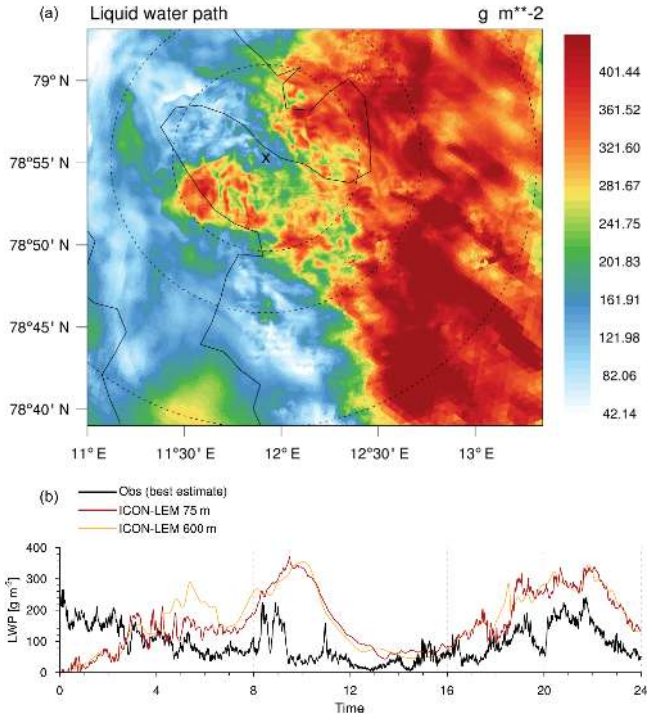

Figure 7. Snapshot of the LWP at 18:30 UTC on 15 June 2017 with an overlay of all four different resolutions, where the dashed lines indicate the size of the different domains, the solid line represents the coast, and the x shows the location of Ny-Ålesund (**a**). An LWP time series for the same day showing the best estimate of the observations and the coarsest (600 m) as well as the finest (75 m) ICON-LEM resolution (**b**).

vations and model output at similar scales is one of the key arguments for high-resolution simulations. Still, questions remain about (i) on which scales variability is resolved by the model and (ii) which resolution is needed to resolve the main part of the observed variability. Figure 7 qualitatively shows how the structure of resolved features becomes finer and more detailed with increasing resolution, i.e., 600, 300, 150 and 75 m from the outer to the inner circles. To quantify this first impression, we calculated the power spectrum of the integrated quantities (LWP, IWV and ice water path (IWP)). Due to data availability, we divided each day into four 6 h parts and picked the sequences with full data availability (see Sect. 2.2 and Fig. 3 for details). For each 6 h time series, we calculated the power density spectrum $P(f_i)$ for the frequencies $F = [\Delta f, \ldots, \frac{1}{2\Delta}]$, where Δ is the smallest time interval of the data set. As the forcing data are produced at a different time frequency, we divided each power density spectrum by the bin width Δf to be independent of the bin width. As the total amount of variance differs between the simulations and the observations and we are interested in the scaling behavior, the power density spectrum has been normalized by the total variance:

$$p(f_i) = \frac{P(f_i)}{\Delta f} \frac{1}{\sum_{f_j \in F} P(f_j)}. \quad (1)$$

Figure 8 shows the normalized power density spectrum for the observations, the four different resolutions of the ICON-LEM and the 2 km ICON-NWP model. Since continuous highly resolved (i.e., here 9 s) IWV and IWP observations are not available, only the retrieved LWP is shown in the analysis. While especially for the forcing data the resolved variability is dominated by the large scales, we see an increase of variability at smaller scales with the four ICON-LEM resolutions. Especially for the 75 m resolution, the model approaches the variability of the observations. While of course the observations also contain a certain amount of noise which might dominate the variability at small scales, it could be an interesting experiment in the future to test even higher model resolutions. For now we see a clear improvement in the representation of the variability at small scales by increasing the resolution from 600 to 75 m.

For IWV and the IWP (see Fig. 8) the behavior is very similar. The highest resolution resolves more energy at smaller scales than the coarser resolutions. While the IWV spectrum decays very quickly with smaller scales, the IWP spectrum decays later, more similarly to the LWP. This shows that the IWV is mainly large-scale driven, while for the IWP and the LWP smaller scales and fluctuations play a more important role, even though the small scales are still partly unresolved by the model as can be seen for the LWP in the comparison with the observations.

5.3 Testing the representativity

The complex terrain around Ny-Ålesund is also a further challenge for point-to-point comparisons between the model and the observations. A slight mismatch in the location of the compared model column might already lead to a completely different environment compared to the observational site. For this reason, we are interested in the questions of how strongly neighboring columns vary and if a point-to-point comparison is meaningful at all. These questions are a subaspect of the long-standing question of how representative measurements at a supersite like Ny-Ålesund are for Arctic regions in general. The model allows us to slowly approach these questions. To show the potential, we take the coarse 2 km ICON simulations and select four different small subregions with different environments (Fig. 9a): the coastal site Ny-Ålesund, sea ice, open water and mixed conditions (where both sea ice and open water occur). For each of these places, we pick 10 neighboring cells and compare the probability density function (PDF) of the LWP of the nine outer cells with the original cell in the center to estimate the local variability. The PDFs are compared based on their mean value and the Hellinger distance, which can also be used to

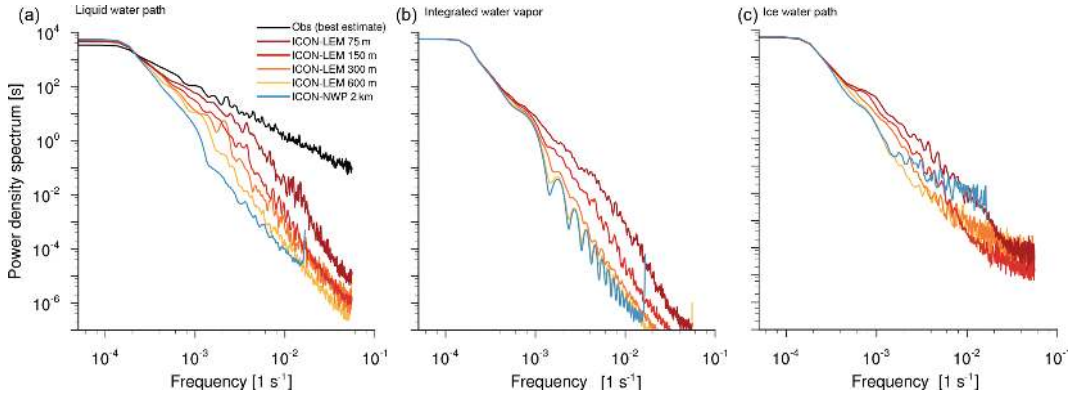

Figure 8. Power density spectrum for the LWP **(a)**, IWV **(b)** and IWP **(c)** according to the ICON-NWP forcing (blue) and the ICON-LEM forcing for the four different resolutions ranging from 600 m (yellow) to 75 m (dark red). For the LWP the observations are also shown (black). The spectrum is averaged over several 6 h time slots excluding 00:00–06:00 UTC every morning due to spin-up and excluding time slots without available observations (see Fig. 3).

compare discrete distributions:

$$H(C,N) = \frac{1}{\sqrt{2}}||\sqrt{C} - \sqrt{N}||_2 = \frac{1}{\sqrt{2}}\sqrt{\sum_{i=1}^{k}(\sqrt{c_i} - \sqrt{n_i})^2}, \quad (2)$$

where $0 \leq H(C,N) \leq 1$, C is the PDF of the original cell and N is the PDF of a single neighboring cell ($N \in \{N_1, \ldots, N_9\}$). For identical distributions, H equals 0. The maximum distance $H = 1$ is achieved for completely disjunct PDFs, which do not overlap.

We see, as could be expected, that the differences of the PDFs are smallest for open water and sea ice conditions. Under mixed conditions close to the fjord, we already see larger differences among the nine grid points, as indicated by a slightly larger Hellinger distance and larger variations in the mean value of the LWP. Clearly, we find the largest Hellinger distance as well as the largest differences in the LWP mean values for the Ny-Ålesund subregion. For a horizontal resolution of approximately 2 km, this is certainly expected, as the neighboring grid cells might be characterized by very different surfaces, e.g., coast, mountains, fjord and glaciers. The larger Hellinger distance and the increased variability of the mean LWP around Ny-Ålesund compared to the other points show that the local features are captured by the model. The point-to-point comparison for Ny-Ålesund certainly has to be performed carefully, but the fact that the local features can be seen by the model is promising in terms of giving a reasonable representation of the column output. In the future, measurements from a scanning MWR can also be used to describe the spatial variability of the LWP and then apply this directly to the context of the model LWP fields. At the moment we can only evaluate the model output at Ny-Ålesund, and the small differences over water or sea ice might also be due to a representation that is too simplistic within the model. Upcoming campaigns (e.g., MOSAiC) will enable us to also evaluate the model under varying conditions, such as over sea ice. The model can thereby be evaluated and tested at observational anchor sites but will provide information on larger domains, e.g., covering the whole Arctic, enabling the comparison of Ny-Ålesund to a larger region.

6 Conclusions

Low-level mixed-phase clouds, which are very common in the Arctic (Shupe et al., 2008), have a substantial impact on the redistribution of radiative energy in the Arctic (e.g., Ebell et al., 2019; Miller et al., 2015) and are driven by very complex processes (Morrison et al., 2012). Thus, their representation is a challenge for today's climate models (Pithan et al., 2014). To improve the respective parameterizations and our process-level understanding, we need tools like a combination of high-resolution models and detailed as well as long-term observations. In this study, we presented the first simulations with the new ICON-LEM under Arctic conditions and over the complex terrain of Ny-Ålesund. We demonstrated its capability to capture the general structure, type and timing of the observed mixed-phase clouds. By analyzing 11 d during the ACLOUD campaign, we showed the potential for more detailed studies focusing on the composition of mixed-phase clouds and the dominating microphysical processes. To understand microphysical processes, it is important to conduct the simulations and the observations on a similar scale, which can only be done with high resolutions. While the overall structure of the observed clouds is already captured in general by large-scale forcing, we showed large differences, especially for the variability of the LWP, between the different resolutions. While a 75 m resolution is also still too coarse for convergence, and higher resolutions might add still more information, we could already see a distinct information gain

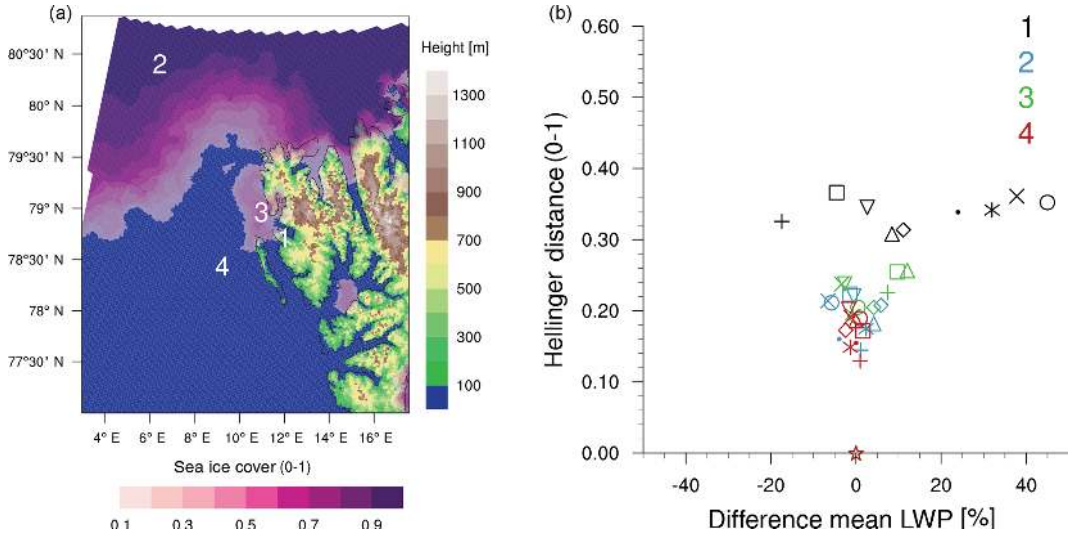

Figure 9. (a) Location of the four 10-grid-point subregions used for the representativity analysis: land (1), sea ice (2), mixed conditions (sea ice and open water, 3) and open water (4). **(b)** The Hellinger distance and differences in the mean LWP of the LWP PDFs of the surrounding grid points (different symbols) compared to the central point (star symbol) of the four subregions (overlaid). Values have been calculated for each day and then averaged over all 11 d.

from the lower ICON resolutions (2000, 600, 300 and 150 m) to the highest ICON resolution (75 m).

For the high-resolution model we chose a rather small domain, which increases dependency on large-scale forcing and thereby also increases the induced uncertainty. Based on a case study, we demonstrated the effect of using two different forcing data sets as well as the benefit of having consistent forcing with a similar model. This consistent forcing can be achieved with the new ICON model suite, which allows simulations on scales reaching from the global scale and climate scales to large-eddy-resolving scales. Even though the parameterizations still have to be exchanged or switched off, the definition of the atmospheric state and the dynamics stay the same, which is a great advantage and reduces both the uncertainty in the high-resolution simulations and the necessary spin-up time.

We found a persistent underestimation of radar reflectivity in the simulations, which hints at particles that are too small and could be due to the CCN and IN background forcing applied. The sensitivity to CCN and IN might be higher toward the poles, especially in the clean Arctic regime, than in the midlatitudes and should be investigated in more detail, including in terms of the ICON-LEM setup.

One long-standing question is the representativity of point measurements in general and especially at complex locations like Ny-Ålesund. We presented a first attempt at showing the potential of high-resolution modeling to tackle these questions by offering a four-dimensional context to the point measurements. In the future, it will be necessary to also evaluate the model under different conditions like sea ice in the central Arctic. Upcoming campaigns like MOSAiC will offer the necessary observational data sets and open up new possibilities for the synthesis of high-resolution modeling and observations in the Arctic.

The presented combination of long-term as well as state-of-the-art observations and the novel ICON model suite, including the ICON-LEM, can lead to improved process understanding and therefore to better representation in models including large-scale models, which will allow us to investigate feedback and climate mechanisms related to Arctic amplification in more detail.

Data availability. ICON-LEM data are available at the long-term archive of the German Climate Computing Center (DKRZ; dataset DKRZ_LTA_1086_ds00001 at http://cera-www.dkrz.de/WDCC/ui/Compact.jsp?acronym=DKRZ_LTA_1086_ds00001, Schemann, 2019). The CloudNet data are available at the CloudNet website (http://devcloudnet.fmi.fi/, Finnish Meteorological Institute, 2019, CloudNet, 2018). The IWV data of the MWR are available at PANGAEA (https://doi.org/10.1594/PANGAEA.902142, Nomokonova et al., 2017).

Author contributions. VS performed the model simulations and the respective analysis of the model output. KE processed the observational data and supported the analysis. Both prepared the manuscript.

Competing interests. The authors declare that they have no conflict of interest.

Special issue statement. This article is part of the special issue "Arctic mixed-phase clouds as studied during the ACLOUD/PASCAL campaigns in the framework of $(AC)^3$ (ACP/AMT inter-journal SI)". It is not associated with a conference.

Acknowledgements. We gratefully acknowledge the funding from the Deutsche Forschungsgemeinschaft (DFG, German Research Foundation), project no. 268020496, TR 172, within the Transregional Collaborative Research Center "ArctiC amplification: Climate Relevant Atmospheric and SurfaCe Processes, and Feedback Mechanisms $(AC)^3$" and the computing time granted on the supercomputer MISTRAL at Deutsches Klimarechenzentrum GmbH (DKRZ) through its Scientific Steering Committee (WLA). We acknowledge the ACTRIS-2 project (European Commission contract H2020-INFRAIA, grant no. 654109) for providing the target classification, which was produced by the Finnish Meteorological Institute using measurements from Ny-Ålesund. We thank Mario Mech for performing the forward simulations with PAMTRA for the model output and Christoph Ritter and Marion Maturilli of the Alfred Wegener Institute, Helmholtz Centre for Polar and Marine Research, Potsdam, for providing MWR and ceilometer data, respectively, used in the CloudNet algorithms. We also thank AWIPEV for hosting the cloud radar of the University of Cologne and the AWIPEV team for helping us with the instrument operation.

Financial support. This research has been supported by the Deutsche Forschungsgemeinschaft (grant no. 268020496).

Review statement. This paper was edited by Radovan Krejci and reviewed by two anonymous referees.

References

Dipankar, A., Stevens, B., Heinze, R., Moseley, C., Zängl, G., Giorgetta, M., and Brdar, S.: Large eddy simulation using the general circulation model ICON, J. Adv. Model. Earth Sy., 7, 963–986, https://doi.org/10.1002/2015MS000431, 2015.

Ebell, K., Nomokonova, T., Maturilli, M., and Ritter, C.: Radiative effect of clouds at Ny-Ålesund, Svalbard, as inferred from ground-based remote sensing observations, J. Appl. Meteorol. Clim., https://doi.org/10.1175/JAMC-D-19-0080.1, 2019.

Finnish Meteorological Institute: CloudNet Classification for Ny-Ålesund, available at: http://devcloudnet.fmi.fi/, last access: 11 December 2019.

Gierens, R., Kneifel, S., Shupe, M. D., Ebell, K., Maturilli, M., and Löhnert, U.: Low-level mixed-phase clouds in a complex Arctic environment, Atmos. Chem. Phys. Discuss., https://doi.org/10.5194/acp-2019-610, in review, 2019.

Goosse, H., Kay, J. E., Armour, K. C., Bodas-Salcedo, A., Chepfer, H., Docquier, D., Jonko, A., Kushner, P. J., Lecomte, O., Massonnet, F., Park, H.-S., Pithan, F., Svensson, G., and Vancoppenolle, M.: Quantifying climate feedbacks in polar regions, Nat. Commun., 9, 1919, https://doi.org/10.1038/s41467-018-04173-0, 2018.

Hande, L. B., Engler, C., Hoose, C., and Tegen, I.: Parameterizing cloud condensation nuclei concentrations during HOPE, Atmos. Chem. Phys., 16, 12059–12079, https://doi.org/10.5194/acp-16-12059-2016, 2016.

Heinze, R., Dipankar, A., Henken, C. C., Moseley, C., Sourdeval, O., Trömel, S., Xie, X., Adamidis, P., Ament, F., Baars, H., Barthlott, C., Behrendt, A., Blahak, U., Bley, S., Brdar, S., Brueck, M., Crewell, S., Deneke, H., Di Girolamo, P., Evaristo, R., Fischer, J., Frank, C., Friederichs, P., Göcke, T., Gorges, K., Hande, L., Hanke, M., Hansen, A., Hege, H.-C., Hoose, C., Jahns, T., Kalthoff, N., Klocke, D., Kneifel, S., Knippertz, P., Kuhn, A., van Laar, T., Macke, A., Maurer, V., Mayer, B., Meyer, C. I., Muppa, S. K., Neggers, R. A. J., Orlandi, E., Pantillon, F., Pospichal, B., Röber, N., Scheck, L., Seifert, A., Seifert, P., Senf, F., Siligam, P., Simmer, C., Steinke, S., Stevens, B., Wapler, K., Weniger, M., Wulfmeyer, V., Zängl, G., Zhang, D., and Quaas, J.: Large-eddy simulations over Germany using ICON: a comprehensive evaluation, Q. J. Roy. Meteor. Soc., 143, 69–100, https://doi.org/10.1002/qj.2947, 2017.

Illingworth, A. J., Hogan, R. J., O'Connor, E. J., Bounoil, D., Brooks, M. E., Delanoë, J., Donovan, P., Eastment, J. D., Gaussiat, N., Goddard, J. W. F., Haeffelin, M., Klein, H., Baltink, H. K., Krasnov, O. A., Pelon, J., Piriou, J.-M., Protat, A., Russchenberg, H. W. J., Seifert, A., Tompkins, A. M., van Zadelhoff, G.-J., Vinit, F., Willén, U., Wilson, D. R., and Wrench, C. L.: CLOUDNET Continous evaluation of cloud profiles in seven operational models using ground-based observations, B. Am. Meteorol. Soc., 88, 883–898, 2007.

Klein, S. A., McCoy, R. B., Morrison, H., Ackerman, A. S., Avramov, A., Boer, G. d., Chen, M., Cole, J. N. S., Del Genio, A. D., Falk, M., Foster, M. J., Fridlind, A., Golaz, J.-C., Hashino, T., Harrington, J. Y., Hoose, C., Khairoutdinov, M. F., Larson, V. E., Liu, X., Luo, Y., McFarquhar, G. M., Menon, S., Neggers, R. A. J., Park, S., Poellot, M. R., Schmidt, J. M., Sednev, I., Shipway, B. J., Shupe, M. D., Spangenberg, D. A., Sud, Y. C., Turner, D. D., Veron, D. E., Salzen, K. v., Walker, G. K., Wang, Z., Wolf, A. B., Xie, S., Xu, K.-M., Yang, F., and Zhang, G.: Intercomparison of model simulations of mixed-phase clouds observed during the ARM Mixed-Phase Arctic Cloud Experiment. I: single-layer cloud, Q. J. Roy. Meteor. Soc., 135, 979–1002, https://doi.org/10.1002/qj.416, 2009.

Küchler, N., Kneifel, S., Löhnert, U., Kollias, P., Czekala, H., and Rose, T.: A W-Band Radar-Radiometer System for Accurate and Continuous Monitoring of Clouds and Precipitation, J. Atmos. Ocean. Tech., 34, 2375–2392, https://doi.org/10.1175/JTECH-D-17-0019.1, 2017.

Loewe, K., Ekman, A. M. L., Paukert, M., Sedlar, J., Tjernström, M., and Hoose, C.: Modelling micro- and macrophysical contributors to the dissipation of an Arctic mixed-phase cloud during the Arctic Summer Cloud Ocean Study (ASCOS), Atmos. Chem. Phys., 17, 6693–6704, https://doi.org/10.5194/acp-17-6693-2017, 2017.

Maahn, M., Löhnert, U., Kollias, P., Jackson, R. C., and McFarquhar, G. M.: Developing and Evaluating Ice Cloud Parameterizations for Forward Modeling of Radar Moments Using in situ Aircraft Observations, J. Atmos. Ocean. Tech., 32, 880–903, https://doi.org/10.1175/JTECH-D-14-00112.1, 2015.

Marke, T., Crewell, S., Schemann, V., Schween, J. H., and Tuononen, M.: Long-Term Observations and High-Resolution

Modeling of Midlatitude Nocturnal Boundary Layer Processes Connected to Low-Level Jets, J. Appl. Meteorol. Clim., 57, 1155–1170, https://doi.org/10.1175/JAMC-D-17-0341.1, 2018.

Maturilli, M. and Kayser, M.: Arctic warming, moisture increase and circulation changes observed in the Ny-Ålesund homogenized radiosonde record, Theor. Appl. Climatol., 130, 1–17, https://doi.org/10.1007/s00704-016-1864-0, 2017.

Maturilli, M., Herber, A., and König-Langlo, G.: Climatology and time series of surface meteorology in Ny-Ålesund, Svalbard, Earth Syst. Sci. Data, 5, 155–163, https://doi.org/10.5194/essd-5-155-2013, 2013.

Maturilli, M., Herber, A., and König-Langlo, G.: Surface radiation climatology for Ny-Ålesund, Svalbard (78.9° N), Theor. Appl. Climatol., 120, 331–339, https://doi.org/10.1007/s00704-014-1173-4, 2015.

Miller, N. B., Shupe, M. D., Cox, C. J., Walden, V. P., Turner, D. D., and Steffen, K.: Cloud Radiative Forcing at Summit, Greenland, J. Climate, 28, 6267–6280, https://doi.org/10.1175/JCLI-D-15-0076.1, 2015.

Morrison, H., de Boer, G., Feingold, G., Harrington, J., Shupe, M. D., and Sulia, K.: Resilience of persistent Arctic mixed-phase clouds, Nat. Geosci., 5, 11–17, 2012.

Neggers, R. A. J., Chylik, J., Egerer, U., Griesche, H., Schemann, V., Seifert, P., Siebert, H., and Macke, A.: Local and remote controls on Arctic mixed-layer evolution, J. Adv. Model. Earth Sy., 11, 2214–2237, https://doi.org/10.1029/2019MS001671, 2019.

Nomokonova, T., Ritter, C., and Ebell, K.: Integrated water vapor of HATPRO microwave radiometer at AWIPEV, Ny-Ålesund, https://doi.org/10.1594/PANGAEA.902142, 2017.

Nomokonova, T., Ebell, K., Löhnert, U., Maturilli, M., Ritter, C., and O'Connor, E.: Statistics on clouds and their relation to thermodynamic conditions at Ny-Ålesund using ground-based sensor synergy, Atmos. Chem. Phys., 19, 410–4126, https://doi.org/10.5194/acp-19-4105-2019, 2019.

Ovchinnikov, M., Ackerman, A. S., Avramov, A., Cheng, A., Fan, J., Fridlind, A. M., Ghan, S., Harrington, J., Hoose, C., Korolev, A., McFarquhar, G. M., Morrison, H., Paukert, M., Savre, J., Shipway, B. J., Shupe, M. D., Solomon, A., and Sulia, K.: Intercomparison of large-eddy simulations of Arctic mixed-phase clouds: Importance of ice size distribution assumptions, J. Adv. Model. Earth Sy., 6, 223–248, https://doi.org/10.1002/2013MS000282, 2014.

Pithan, F., Medeiros, B., and Mauritsen, T.: Mixed-phase clouds cause climate model biases in Arctic wintertime temperature inversions, Clim. Dynam., 43, 289–303, https://doi.org/10.1007/s00382-013-1964-9, 2014.

Schemann, V.: Cloud variables from ICON-LEM around Ny-Aalesund, available at: http://cera-www.dkrz.de/WDCC/ui/Compact.jsp?acronym=DKRZ_LTA_1086_ds00001, last access: 19 December 2019.

Screen, J. A., Deser, C., Smith, D. M., Zhang, X., Blackport, R., Kushner, P. J., Oudar, T., McCusker, K. E., and Sun, L.: Consistency and discrepancy in the atmospheric response to Arctic sea-ice loss across climate models, Nat. Geosci., 11, 155–163, https://doi.org/10.1038/s41561-018-0059-y, 2018.

Seifert, A. and Beheng, K. D.: A two-moment cloud microphysics parameterization for mixed-phase clouds. Part 1: Model description, Meteorol. Atmos. Phys., 92, 45–66, https://doi.org/10.1007/s00703-005-0112-4, 2006.

Serreze, M. C. and Barry, R. G.: Processes and impacts of Arctic amplification: A research synthesis, Global Planet. Change, 77, 85–96, https://doi.org/10.1016/j.gloplacha.2011.03.004, 2011.

Shupe, M. D., Matrosov, S. Y., and Uttal, T.: Arctic Mixed-Phase Cloud Properties Derived from Surface-Based Sensors at SHEBA, J. Atmos. Sci., 63, 697–711, https://doi.org/10.1175/JAS3659.1, 2006.

Shupe, M. D., Daniel, J. S., DeBoer, G., Eloranta, E. W., Kollias, P., Long, C. N., Luke, E. P., Turner, D. D., and Verlinde, J.: A focus on mixed-phase clouds, B. Am. Meteorol. Soc., 89, 1549–1562, 2008.

Tjernström, M., Shupe, M. D., Brooks, I. M., Achtert, P., Prytherch, J., and Sedlar, J.: Arctic Summer Airmass Transformation, Surface Inversions, and the Surface Energy Budget, J. Climate, 32, 769–789, https://doi.org/10.1175/JCLI-D-18-0216.1, 2019.

Wendisch, M., Brückner, M., Burrows, J. P., Crewell, S., Dethloff, K., Ebell, K., Lüpkes, C., Macke, A., Notholt, J., Quaas, J., Rinke, A., and Tegen, I.: Understanding causes and effects of rapid warming in the Arctic, EOS, 98, 22–26, https://doi.org/10.1029/2017EO064803, 2017.

Wendisch, M., Macke, A., Ehrlich, A., Lüpkes, C., Mech, M., Chechin, D., Dethloff, K., Velasco, C. B., Bozem, H., Brückner, M., Clemen, H.-C., Crewell, S., Donth, T., Dupuy, R., Ebell, K., Egerer, U., Engelmann, R., Engler, C., Eppers, O., Gehrmann, M., Gong, X., Gottschalk, M., Gourbeyre, C., Griesche, H., Hartmann, J., Hartmann, M., Heinold, B., Herber, A., Herrmann, H., Heygster, G., Hoor, P., Jafariserajehlou, S., Jäkel, E., Järvinen, E., Jourdan, O., Kästner, U., Kecorius, S., Knudsen, E. M., Köllner, F., Kretzschmar, J., Lelli, L., Leroy, D., Maturilli, M., Mei, L., Mertes, S., Mioche, G., Neuber, R., Nicolaus, M., Nomokonova, T., Notholt, J., Palm, M., van Pinxteren, M., Quaas, J., Richter, P., Ruiz-Donoso, E., Schäfer, M., Schmieder, K., Schnaiter, M., Schneider, J., Schwarzenböck, A., Seifert, P., Shupe, M. D., Siebert, H., Spreen, G., Stapf, J., Stratmann, F., Vogl, T., Welti, A., Wex, H., Wiedensohler, A., Zanatta, M., and Zeppenfeld, S.: The Arctic Cloud Puzzle: Using ACLOUD/PASCAL Multiplatform Observations to Unravel the Role of Clouds and Aerosol Particles in Arctic Amplification, B. Am. Meteorol. Soc., 100, 841–871, https://doi.org/10.1175/BAMS-D-18-0072.1, 2019.

Zängl, G., Reinert, D., Rípodas, P., and Baldauf, M.: The ICON (ICOsahedral Non-hydrostatic) modelling framework of DWD and MPI-M: Description of the non-hydrostatic dynamical core, Q. J. Roy. Meteor. Soc., 141, 563–579, https://doi.org/10.1002/qj.2378, 2015.